European Congress on Computational Methods in Applied Sciences and Engineering
Eccomas 2000
Barcelona, 11-14 September 2000

COMPRESSIVE FAILURE, LARGE-STRAIN DUCTILITY AND SIZE EFFECT IN CONCRETE: MICROPLANE MODEL

Zdeněk P. Bažant* **and Michele Brocca***

*Department of Civil Engineering, Northwestern University, Evanston, IL 60208-3109, USA
e-mail: z-bazant@nwu.edu

Keywords: Concrete, ductility, size effect, scaling, compressive failure, fracture, finite element analysis, microplane model.

Abstract. The paper presents applications of the microplane model for concrete in finite element analyses performed to investigate two aspects of the compressive behavior of concrete. The first aspect is the ductile response, observed under extreme pressures, and the second aspect is the quasibrittle response, exhibited under normal pressures. Pressures high enough to induce ductile response are developed, for instance in impact events, and the ductile properties of concrete at high pressures can be observed in the "tube-squash" test, conceived at Northwestern University, in which concrete is cast inside a thick steel tube. In such a test the confinement provided by the steel tube allows concrete to achieve very large deviatoric strains (with shear angles up to 70°), retaining integrity, without visible damage. The axial compression of the tube filled with concrete is reproduced with a finite strain, finite element analysis, proving the capability of the microplane model for concrete to capture accurately the behavior of concrete under extreme pressures. In conditions of normal confinement, concrete exhibits quasibrittle behavior in compression, resulting in a significant size effect in the compressive failure of concrete structures. Finite element simulations of the compressive failure of reduced-size columns show good agreement with the structural response observed experimentally. For the latter analysis, the microplane constitutive law is employed adopting the crack band model.

1 INTRODUCTION

The mechanical behavior of concrete in compression is complex and highly pressure-sensitive. Under low hydrostatic pressure, concrete typically behaves in compression as a quasi-brittle material. However, under high hydrostatic pressures (1~2 × compressive strength) the response becomes plastic and concrete can achieve very large deviatoric deformations without exhibiting visible cracking or damage.

A thorough understanding and accurate modeling of the behavior of concrete in compression is necessary to perform finite element simulations of the mechanical response of concrete structures. In particular, extremely high hydrostatic pressures are attained during impact events such as missile penetration and explosive driving of anchors. Rather high pressures may be cause by blast or seismic loading. On the other hand an accurate description of the quasibrittle behavior of concrete at low pressures is essential to reproduce the size effect, which is observed in the compressive failure of concrete structures.

An efficient and accurate constitutive model for concrete has been developed by Bažant and coworkers[1-8] over the past two decades within the numerical and theoretical framework of the microplane model. The microplane model is employed here for the finite element simulation of tests exhibiting ductile behavior under high pressures and size effect. The accuracy of the numerical present results further atests the validitity of the microplane model for concrete, which was already shown to yield excellent results at moderate pressures or tension for a broad range of triaxial loading conditions.

The paper is organized as follows: Section 2 reviews the general concepts and formulation of the microplane model; the microplane model for concrete is briefly presented in section 3; section 4 presents the experimental results and numerical analysis of the 'tube-squash' test; and section 5 focuses on the study of the size effect in compressive failure of concrete columns. The paper closes by a concise discussion in section 5.

2 THE MICROPLANE MODEL

With the microplane model approach [1-9], the constitutive behavior of materials is characterized by relations between the stress and strain vectors acting on planes of all possible orientations within the material (microplanes), and the macroscopic strain and stress tensors are determined by considering the contribution of the stress and strain components on all the planes.

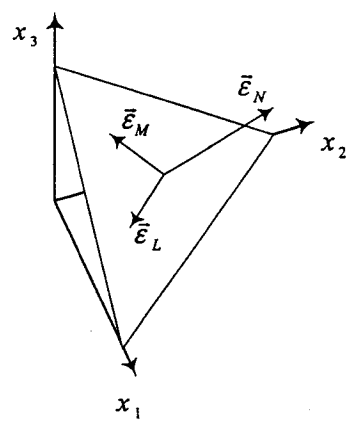

Fig. 1- Components of strain on a microplane

The orientation of a microplane is characterized by the unit normal **n** of components n_i (indices i and j refer to the components in Cartesian coordinates x_i). The microplane can be constrained to the macroscopic strain tensor ε_{ij} kinematically of statically. In the formulation with kinematic constraint, which makes it possible to describe softening in a stable manner, the strain vector $\vec{\varepsilon}_N$ on the microplane (Figure 1) is the projection of ε_{ij}. So the components of this vector are $\varepsilon_{Ni} = \varepsilon_{ij} n_j$. The normal strain on the microplane is $\varepsilon_N = n_i \varepsilon_{Ni}$, that is

$$\varepsilon_N = N_{ij} \varepsilon_{ij}; \qquad N_{ij} = n_i n_j \tag{1}$$

where repeated indices imply summation over i = 1,2,3. The mean normal strain, called the volumetric strain ε_V, and the deviatoric strain ε_D on the microplane can also be introduced, defined as follows (for small strains):

$$\varepsilon_V = \varepsilon_{kk}; \qquad \varepsilon_D = \varepsilon_N - \tfrac{1}{3}\varepsilon_V = \tfrac{2}{3}(\varepsilon_N - \varepsilon_S) \tag{2}$$

where ε_S = spreading strain = mean normal strain in microplane. ε_S characterizes the lateral confinement of the microplane and the creation of splitting cracks normal to the microplane. Considering ε_V and ε_D (or ε_S) is useful when dealing with the effect of lateral confinement on compression failure and when the volumetric-deviatoric interaction observed for a number of cohesive frictional materials, such as concrete, needs to be captured.

To characterize the shear strains on the microplane (Figure 1), we need to define two coordinate directions M and L, given by two orthogonal unit coordinate vectors **m** and **l** of components m_i and l_i lying on the microplane. To minimize directional bias of **m** and **l** among microplanes, we alternate among choosing vectors **m** to be normal to axis x_1, x_2 or x_3.

The magnitudes of the shear strain components on the microplane in the direction of **m** and **l** are $\varepsilon_M = m_i(\varepsilon_{ij} n_j)$ and $\varepsilon_L = l_i(\varepsilon_{ij} n_j)$. Because of the symmetry of tensor ε_{ij}, the shear strain components may be written as follows (e.g. [5]):

$$\varepsilon_M = M_{ij} \varepsilon_{ij}; \qquad \varepsilon_L = L_{ij} \varepsilon_{ij} \tag{3}$$

in which the following symmetric tensors are introduced:

$$M_{ij} = (m_i n_j + m_j n_i)/2; \qquad L_{ij} = (l_i n_j + l_j n_i)/2 \tag{4}$$

Once the strain components on each microplane are obtained, the stress components are updated through microplane constitutive laws, which can be expressed in algebraic or differential form.

If the kinematic constraint is imposed, the stress components on the microplanes are equal to the projections of the macroscopic stress tensor σ_{ij} only in some particular cases, when the microplane constitutive laws are specifically prescribed so that this condition be satisfied. This happens for example in the case of elastic laws at the microplane level, defined with elastic constants chosen so that the overall macroscopic behavior is the usual elastic behavior [9].In general, the stress components determined independently on the various planes will not be

related to one another in such a manner that they can be considered as projections of a macroscopic stress tensor. Thus static equivalence or equilibrium between the microlevel stress components and macrolevel stress tensor must be enforced by other means. This can be accomplished by application of the principle of virtual work, yielding

$$\sigma_{ij} = \frac{3}{2\pi}\int_{\Omega}\sigma_N n_i n_j \mathrm{d}\Omega + \frac{3}{2\pi}\int_{\Omega}\frac{\sigma_{Tr}}{2}(n_i\delta_{rj} + n_j\delta_{ri})\mathrm{d}\Omega \qquad (5)$$

where Ω is the surface of a unit hemisphere. Equation (5) is based on the equality of the virtual work inside a unit sphere and on its surface, rigorously justified in Bažant et al. [10].

The integration in Equation (5), is performed numerically by an optimal Gaussian integration formula for spherical surface using a finite number of integration points on the surface of the hemisphere. Such an integration technique corresponds to considering a finite number of microplanes, one for each integration point. A formula consisting of 28 integration points is given by Stroud [11]. Bažant and Oh [10] developed a more efficient and about equally accurate formula with 21 integration points, and studied the accuracy of various formulas in different situations.

3 THE MICROPLANE MODEL FOR CONCRETE

The microplane model for concrete is the result of almost two decades of studies by Bažant and coworkers. The version adopted for the analyses presented in this paper is referred to as M4 and a complete description of it can be found in Bažant et al. [5-8].

The model is formulated by use of simple one-to-one relations between one stress component and the associated strain component. Except for a frictional yield surface, cross dependencies are not accounted for explicitly, but appear in the model as result of the interaction among planes.

Each constitutive relationship at the microplane level is expressed by introducing stress-strain boundaries (strain independent yield limits): the response is elastic until any of the boundaries is reached; after that, the stress drops at constant strain to the boundary.

The model parameters are divided into a few adjustable ones (only four are needed) and many nonadjustable ones(of which twenty are used), common to all concretes. Bažant et al. [7] provide an efficient procedure to identify the model parameters in a systematic way from test data. Creep and rate-effect have also been introduced in M4, but are neglected in this study.

4 THE SQUASH TEST

4.1 Presentation of the test

The tube-squash test is a new type of test developed at Northwestern University [12], which allows the investigation of the mechanical behavior of concrete under very high hydrostatic pressures into the finite strain range. The concrete specimen is cast inside a tube made of a highly ductile steel alloy, capable of large deformation, up to 100%, without cracking. After curing, the tube is then squashed up to one half of its original length, causing the specimen to bulge.

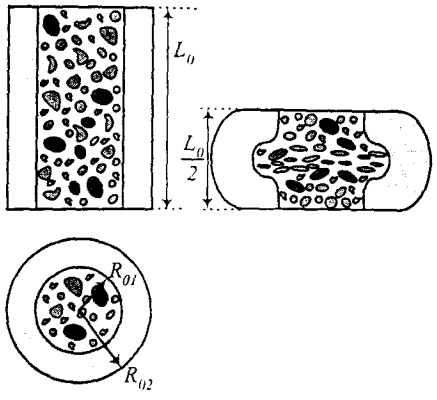

Fig. 2 The specimen for the squash test. Steel tube filled with concrete.

Fig. 2 shows the cross sections of one of the specimens used for the test, as it appears at the beginning and at the end of the test, after the loading process. Figs. 3-4 show a schematic drawing and two pictures of the experimental set up used for the test.

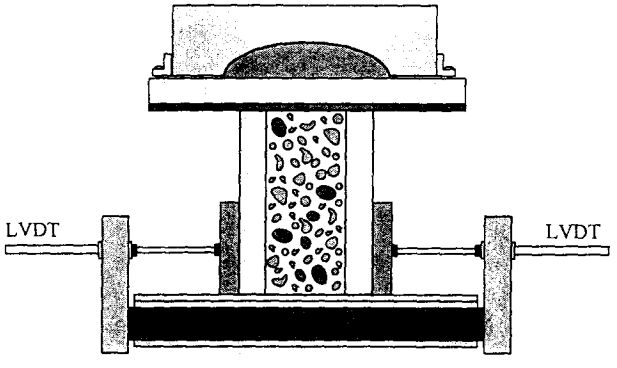

Fig. 3 Experimental set up for the squash test.

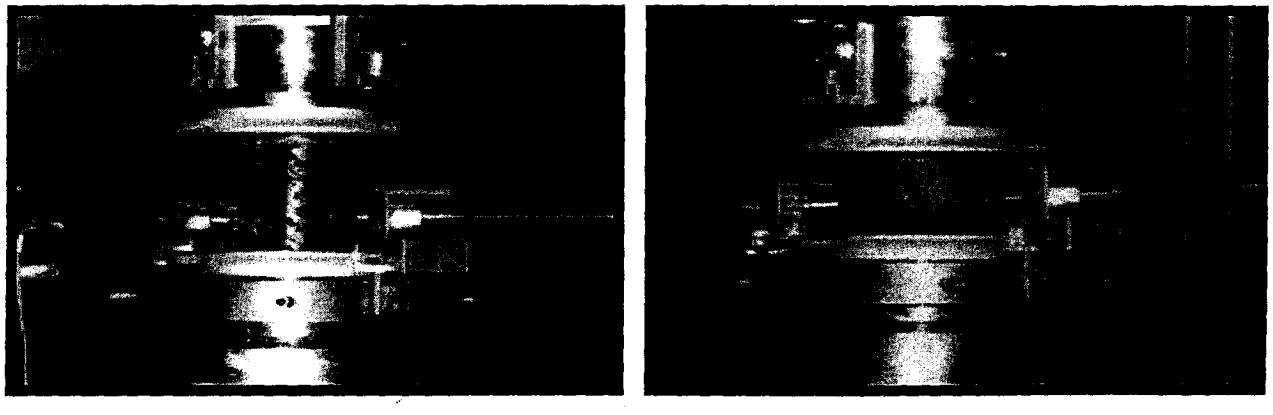

Fig. 4 Pictures of the experimental set up for the squash test.

During the loading process, concrete inside the tube is subjected to extremely large strains while retaining its integrity (Fig. 5). No visible damage, cracks or voids can be observed inside the concrete mass at the end of the test. Some damage however occurs in concrete at the microscopic level, as manifested by a reduction of Young's modulus, tensile strength and compressive strength after the test (all these quantities are reduced to approximately one third of their original value). The previous triaxial tests and confined uniaxial-strain compression tests achieve high pressures, but they cannot achieve large strains, neither shear nor normal. The tube-squash test can achieve very high normal strains and shear (or deviatoric) strains by allowing the specimen to deform highly nonuniformly. The penalty is a more complicated identification of the constitutive relation. The large deformations as well as stresses inside the concrete volume would be hard to measure and so they are not. To keep the test inexpensive and easy to perform, only a limited set of data are measured. The quantities measured during the test are the axial displacement under the load, the axial applied load and the lateral displacement of the tube at mid-height. Also the final shape of the specimen is recorded at the end of the test, after the specimen is cut longitudinally, in order to observe the inner profile assumed by the steel tube after deformation. Information about the stress and strain fields may be deduced from these data.

Two specimen sizes have been tested: tubes of diameter of 76.2 mm (3.0 in.) and 63.5 mm (2.5 in.). The wall thickness is 14.22 mm (0.56 in.) and 12.7 mm (0.5 in.) respectively. The length of the tube is 88.9 mm (3.5 in.) in both cases.

Tests have been conducted on tubes filled with normal strength and high strength concrete, hardened Portland cement paste and cement mortar, and on tubes with a snugly fitted limestone insert. All the specimens show remarkable plastic behavior under extreme deformation. This study considers only high strength concrete specimens, cast inside the smaller tubes (diameter 63.5 mm, thickness 12.7 mm).

As a companion test, also the empty steel tube is squashed in the same manner. The data obtained from testing the steel alone can be used to calibrate a material model for steel. This process is crucial, since a good accuracy is required in the analysis of the behavior of steel during the squash test.

Fig. 5 Cross sectional photograph of a high strength concrete filled tube and of an empty steel tube after the test.

Fig. 5 is a cross sectional photograph of a high strength concrete filled tube and of an empty steel tube specimen after 50 % axial shortening. Note how the inner profile of the deformed steel tube is affected by the presence of concrete.

4.2 Numerical results

The hardening parameters employed in the model for steel are tuned using the results of the companion test on the empty steel tube. Fig. 6 shows a three dimensional visualization of the mesh used for the analysis of the steel tube and the deformed mesh at the end of the process. Fig. 7 shows a comparison of the experimental load displacement diagram with the one obtained by finite element analysis. Clearly the material parameters can be adjusted so that the experimental curve is fitted very accurately.

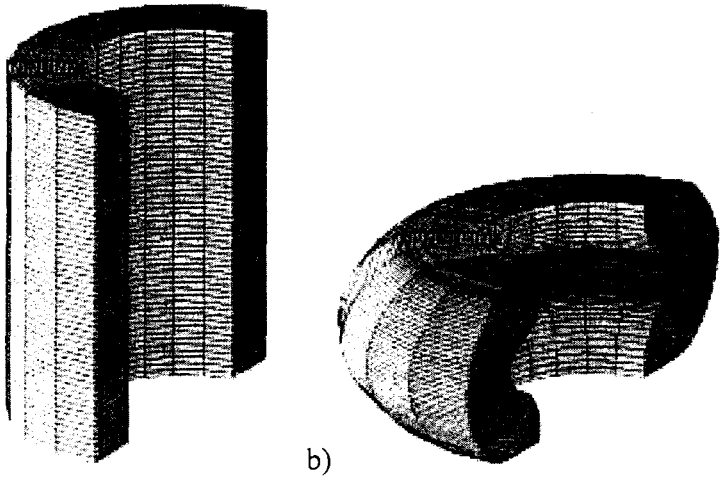

Fig. 6- Three-dimensional visualization of the mesh used for the analysis on the empty tube. a) Undeformed, and b) at the end of the loading process.

The results of the analysis of the concrete filled tube are shown in the following figures. Fig. 8 shows the initial and deformed mesh and Fig. 9 gives the load displacement curve. In this case it was sufficient to adjust merely the parameter controlling the compressive strength in the microplane model for concrete in order to reproduce very closely the mechanical behavior of the specimen observed experimentally. That no other adjustments were needed is remarkable.

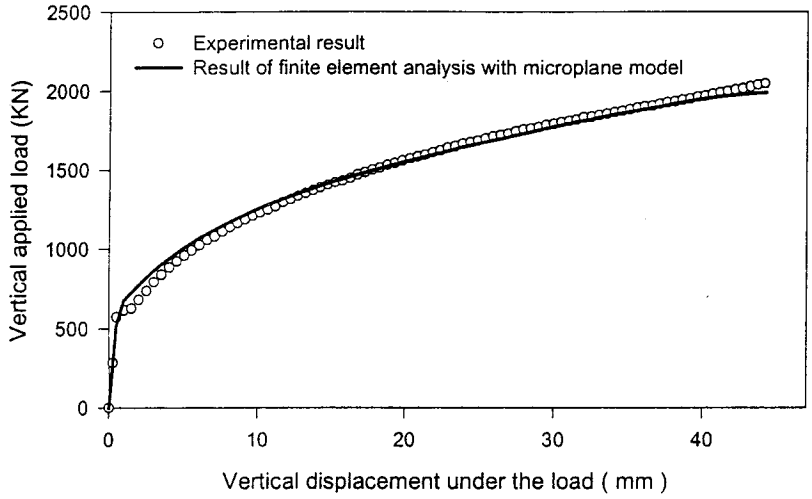

Fig. 7- Experimental and computed load-displacements diagram for the empty tube.

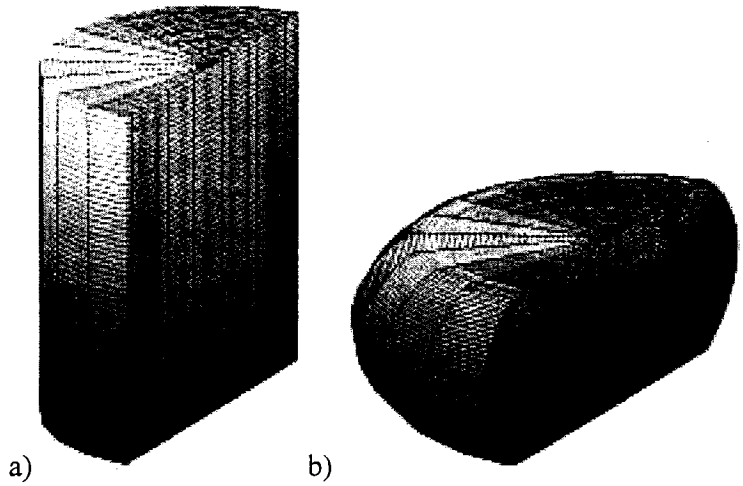

Fig. 8- Three-dimensional visualization of the mesh used for the analysis on the tube filled with concrete. a) Undeformed, and b) at the end of the loading process.

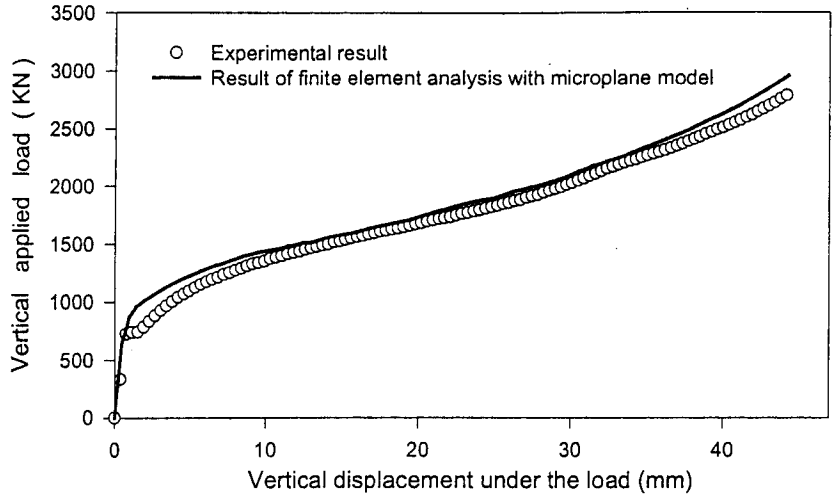

Fig. 9- Experimental and computed load-displacements diagram for the tube filled with concrete.

Fig. 10 shows the radial stress in concrete calculated at three different distances from the axis of the specimen.

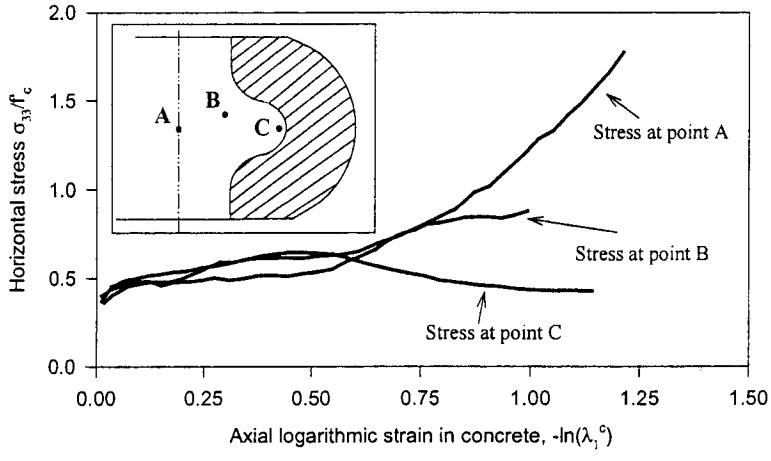

Fig. 10- Computed radial compressive stress in concrete at three different points.

At the axis, the radial stress reaches about $1.8 f_c$, while the axial stress is about $8 f_c$, and the volumetric (hydrostatic) stress component is about $3.9 f_c$.

The maximum shear angle, which occurs at point A, is obtained for the end of the test as 71.5°. The simplified analysis in Bažant et al. [12] led to the estimate of 70°, which is very close.

5 SIZE EFFECT IN COMPRESSIVE FAILURE OF CONCRETE COLUMNS

Current design codes, based on failure criteria expressed in terms of strength or yield surfaces, exhibit no size effect, i.e. no dependence of the nominal strength on the size of the structure. However the failure of concrete columns is not plastic, but brittle, as confirmed by the fact that the observed load deflection diagrams of columns have no yield plateau but descend after the peak. As seen in the preceding section, under extremely high confining pressures, compressive failure of concrete can be ductile, without any significant post-peak decrease of applied load, but such pressures can be developed only when the concrete is confined in very strong steel tubes. Thus description of structural behavior of concrete in terms of plastic limit states is in general not correct. Mathematical modeling of such behavior should be based on fracture mechanics, which predicts size effect, such that the nominal strength at failure, σ_N, decreases with increasing of the characteristic dimension of the structure, D, provided that the structures of different sizes are geometrically similar.

It is now recognized that size effects must occur in all the failures of concrete structures that are due to concrete rather than to steel except when concrete is at extreme hydrostatic pressures. This is true not only of those failures that are due to concrete failing in tension (diagonal shear, punching shear, torsion, anchor pullout, bar pull-out, splice fracture, etc.) but also of the failures that are due to concrete failing in compression. This includes bending fgailures of prestressed concrete beams, anchor of bar pullout, diagonal shear failure of reinforced concrete beams, punching shear and torsion, in fact, all the cases analyzed by the strut-and-tie model in which failure is due to crushing of the compression strut of concrete. Most importantly, this includes reinforced concrete columns, which will be studied in this paper from the size effect viewpoint.

Studies reporting size effect in compressive failure of quasibrittle materials such as concrete, rock, ceramics and composites can be found, e.g., in van Mier [13], Gonnermann [14], Blanks and McNamara [15], Marti [16], and Jishan and Xixi [17].

Although important advances have been made in the past in the understanding of reinforced concrete columns (see e.g. Nilson and Winter [18], and for further references consult McGregor [19], Bažant and Cedolin [20], and Bažant and Xiang [21]), the size effect in columns has escaped attention so far.

Until about 15 years ago, it had been erroneously believed that all the size effects in concrete structures are totally explicable by the statistical nature of material strength as described by Weibull-type theories. In reality, however, the portion of the size effect ascribable to the randomness of concrete strength is very small and negligible in structures in which there is large crack growth before the maximum load is reached (Bažant [22]; Bažant et al. [23]; Bažant and Xi [24]). In such structures, the size effect is almost totally deterministic and is caused by the fact that a larger structure stores a greater amount of strain energy and thus the rate of energy release into an advancing fracture front grows is larger for a larger structure, while the energy dissipated at the fracture front per unit fracture advance is approximately independent of the structure size. This source of size effect in concrete was originally recognized [38] for the case of tensile failure , but a similar phenomenon occurs also when the structure fails in compression.

Compressive failure is caused predominantly by the release of stored energy from the structure in a fashion similar to tensile failure as suggested and implied by several researchers (e.g., Ingraffea [25]; Bažant et al. [26]; Bieniawski [27]; Hoek and Bieniawski [28]; Cotterell [29]; Paul [30]). Therefore the study of size effect in compression must be based on fracture mechanics. A simplified model for the mechanism of compression failure, aimed at the study of the accompanying size effect, is given by Bažant and Xiang [31], who modeled the propagation of a cracking band assumed to consist of densely distributed axial splitting microcracks.

The objective of this section is to show how size effect in concrete columns can be determined through a finite element analysis based on the crack-band concept. This will be done by performing a finite element analysis of a series of laboratory tests conducted at Northwestern University (Bažant and Kwon [32]).

5.1 Presentation of experimental results

In 1994, Bažant and Kwon[32] presented the results of a series of tests performed on reinforced concrete columns of reduced size made with microconcrete. The purpose of these tests was to show the presence of a significant size effect in compressive failure of columns, and to ascertain how the strengths of columns of different sizes are mutually related.

The test specimens (Fig. 11) were tied reinforced concrete columns of square cross sections with sides D = 12.7, 25.4 and 50.8 mm (0.5, 1 and 2 in.). Three column slendernesses λ = 19.2, 35.8 and 52.5, were used; $\lambda = L/r$, and according to ACI, $r = 0.3D$ (for typical reinforced concrete sections). The corresponding effective lengths of the columns, measured between the contact points of the steel balls, were L= 73, 136.5 and 200 mm (2.875, 5.375 and 7.875 in.) for the smallest cross section, L =146, 273 and 400 mm (5.75, 10.75 and 15.75 in.) for the middle cross section, and L = 292, 546 and 800 mm (11.5,21.5 and 31.5 in.) for the largest cross section. The loads were applied to the steel platens through steel balls and steel plates.

In each group, the columns of the same slenderness and different cross sections were geometrically similar. The geometric similarity was enforced scrupulously: the reinforcing bars, their location coordinates and cover, as well as the diameter and spacing of the ties were all scaled in proportion to D.

The columns were simply supported and the load P was applied with eccentricities e which were geometrically similar: $e = 0.25D$. The steel ratio was 4.91%. The Young's modulus of the steel bars was E_s = 200 GPa (29 000 ksi) and the yield strength was f_y = 552 Mpa (80 000 psi).

The concrete (actually a microconcrete or mortar) was made of Type I Portland cement with water/cement ratio 0.65 (for easy workability). The maximum aggregate size was 3.35 mm (0.132 in.). All the specimens were cast from the same batch of concrete. The average uniaxial compression strength of concrete was f_c' = 28.96 MPa (4200 psi). Note that the aggregate size d_a was kept constant and not scaled with size D. This must be so because, if d_a were changed, one would have a different concrete, with different properties. The known scaling laws for geometrically similar structures of different sizes are valid only when one and the same material is used for all the sizes.

The results of the tests are shown in Fig. 15, on plots of σ_N versus log D, which represent the standard size effect plots. The value of the nominal strength $\sigma_N = P/D^2$ is calculated from the peak loads measured in individual tests. All these plots clearly indicate a strong size effect.

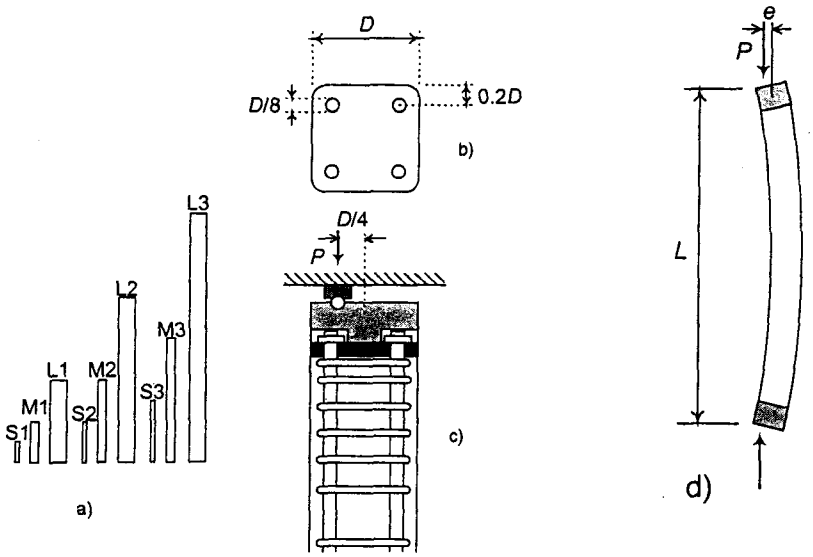

Fig. 11- Tests on columns of different size and slenderness.

5.2 Numerical results

The finite element analysis of the tests presented in the previous sub-section is performed using a three-dimensional explicit finite element code developed with updated Lagrangian formulation. Eight-node brick elements are used for concrete and for the steel plates at the top and bottom of the specimen. The reinforcement is modeled with truss elements, and an elastic-plastic law is assumed for steel. Debonding of reinforcing bars is neglected. Note that the assumption of perfect bond between concrete and steel is a simplification that might have some effect on the results. This point will be discussed further.

The constitutive law adopted for concrete is the microplane model M4. In microplane finite element analysis, damage is modeled as smeared over the domain of the element. When such a smeared approach is used, numerical analysis of compression failure of concrete faces the same difficulties as posed by tensile strain softening in quasi-brittle failure. The softening behavior included into the constitutive law might cause loss of well-posedness and spurious strain localization into arbitrarily small regions.

This can be easily understood by considering the example of a bar made of a material characterized by an elastic-softening constitutive law (see e.g. Bažant [33, 38]; Bažant and Planas [34]). If the bar is discretized into N elements, it can be shown that, after the stress peak, the strain must localize in only one of the elements. Only one element continues stretching, while the others unload elastically [38]. Thus the size of the damaged region and the post-peak response of the bar depend on N. Such phenomenon is usually referred to as mesh unobjectivity or spurious mesh sensitivity and is obviously unacceptable - conceptually, physically and computationally.

The only known satisfactory remedy of this problem is to apply a nonlocal continuum concept in some form to the strain softening damage. In a nonlocal formulation, it is recognized that continuum damage models cannot be implemented with the classical assumption that stress at a point depends only on the strain at the same point. Rather, a more general concept of nonlocal continuum must be adopted, according to which the stress at a point depends also on the

strain in the neighborhood of that point, or on some type of average of strain in the neighborhood (this average may futher be approximated by the second strains gradient). By doing so, the nonlocal approach can account for the interaction of microcracks and other microscale sources of damage.

However, even without directly addressing nonlocality, spurious strain localization can be prevented by introducing some type of *strain localization limiter*, i.e. a mathematical restriction on the size of the damaged region to be associated to the material constitutive model. A popular and effective way to do so is the crack band model, introduced in general terms by Bažant [33, 38] and developed in full detail for sudden cracking in Bažant and Cedolin and Cedolin and Bažant, and for gradual strain softening Bažant and Oh [35].

The basic idea in the crack band model is that the damage propagates as a band whose width has a certain characteristic value h_c. For a given constitutive law of concrete, h_c depends on the strain-softening curve. The element size must be determined accordingly. In most cases, when the damage region (crack band) propagates inside a finite element mesh, its width will be equal to the size of the elements in the direction perpendicular to the direction of propagation of the damage. Therefore the element size in such a direction must be equal to h_c.

The crack band approach has been introduced and extensively used for analysis of tensile fracture. As already mentioned, the propagation of a region of compressive strain-softening damage is driven by energy release in the structure and, in this sense, it is a phenomenon analogous to the propagation of tensile cracking. Thus in terms of strain localization, the same arguments as those made when dealing with tensile failure apply also to the case of compressive failure.

Determining the proper band width (and thus the element size) to be adopted in finite element analysis is not a simple task. Often this must be done empirically. There is no sufficient previous experience available to tell what is the optimum element size for a computation with the microplane model. For the analysis of concrete columns presented in this paper, the element size was empirically determined as the element size that gives accurate results for one of the 9 specimens to be analyzed (namely the small specimen of intermediate slenderness, S2), and has been kept constant for the remaining computations. This guarantees consistency throughout the analysis and makes possible a meaningful comparative study of the results obtained for different specimen sizes. The element size in the direction normal to the expected plane of propagation of the damage region (the horizontal plane) is taken to be approximately 1.7 times the aggregate size.

One last comment needs to be made on the effect that the orientation of the elements in the mesh might have on the results. Whenever a damage region propagates through the elements of a finite element mesh, there is a tendency for it to follow the mesh lines. A comparison of results obtained for different meshes, with different orientation of the elements, would be needed, in order to capture accurately the propagation of the damage into the column. However, the main focus of this paper is on the size effect and thus, during each computation, what is needed is the nominal strength, $\sigma_N = P/D^2$, calculated from the peak load. The peak is reached when the reinforcing bars buckle, after softening of the surrounding concrete. Therefore, at peak, the damage region has not propagated deep inside the column. For this reason, the mesh adopted for the computation seems to be sufficient to capture the response of the columns up to the peak. A

correct prediction of the propagation of the damage would be essential to capture accurately the post-peak structural behavior of the column, which is beyond the scope of this paper.

Fig. 12-14 show the meshes used for specimens of three slendernesses. Each figure exhibits three specimens with the same cross section and three different slendernesses. For each specimen type, the figure shows separately the finite elements used to model the reinforcement (including top and bottom steel plates), the undeformed mesh of the whole specimen and the deformed mesh at the end of the loading process. The specimen sizes (cross section sides) are D = 12.7, 25.4 and 50.8 mm (0.5, 1 and 2 in.) for Fig. 12, 13 and 14 respectively.

The size effect is determined by comparing the results obtained for geometrically similar specimens with constant slenderness λ and varying size D . The best way to discuss systematically the results of finite element analysis is, however, by plotting them on standard size effect plots of $\log \sigma_N$ versus $\log D$. Such plots are shown in Fig. 15, for the three groups of specimens, again grouped by slenderness.

Based on previous theoretical arguments of general validity [see Bažant and Cedolin [20], Chapter 12 and 13, or Bažant and Kazemi [36], Bažant [37]], the size effect should be described by the following approximate size-effect law proposed by Bažant [38]:

$$\sigma_N = Bf_t'(1+\beta)^{1/2}, \qquad \beta = D/D_0 \tag{6}$$

in which Bf_t' and β are two empirical constants (the tensile strength f_t', is introduced merely for convenience, to make B non-dimensional). For comparison, Fig. 5.5 shows also the experimental results and their optimal fits by this size effect law.

Experimental evidence and theoretical arguments (see, e.g. Bažant and Planas [34]) show that the dependence of $\log \sigma_N$ on $\log D$ for geometrically similar structures is such that it approaches a horizontal asymptote for small sizes and a straight line asymptote of slope –1/2 for D→ ∞. For D → ∞, the size of the fracture process zone, compared to the size of the structure, is so small that the behavior of the structure approaches that predicted by linear elastic fracture mechanics. When the result of finite element analysis are shown in the bilogarithmic plot, it can be seen that a smooth curve interpolating the three points for the three specimen sizes has negative curvature, in agreement with the theory. This shows that the size effect is captured in a realistic way.

Quantitatively the results are satisfactory too, although the predicted size effect is less strong than that observed experimentally. In particular, observe that the approximation seems to worsen slightly with increasing slenderness. There are two reasons to which this discrepancy can be attributed. In the first place, the present analysis assumes perfect bond between steel bars and concrete. The steel bars used in the test are smooth, as explained in section 2, and therefore debonding and pull out might have played some role in reducing the nominal strength with increasing size. Obviously, debonding cannot be captured under the assumptions made for the present analysis. Second, the constitutive model used in the computation is local. The crack band model gives results too stiff because the mesh could not be laid out so that the mesh lines would follow the boundary of the softening damage zone (this is known as "stress locking"). Also the crack band model cannot distinguish the mutual amplification and shielding crack interaction. Doubtless, a non-local formulation, using finite elements at least three times smaller would yield more accurate results. However, the number of finite elements required would increase 27-times, which would call for a more powerful computer than that affordable for this project.

Size effect testing of real size columns with real size aggregates has also begun (Abusiaf et al. [39]). The results so far agree with Bažant and Xiang's analysis [31]. However, they are limited in the range and scope to serve as a check on the present model.

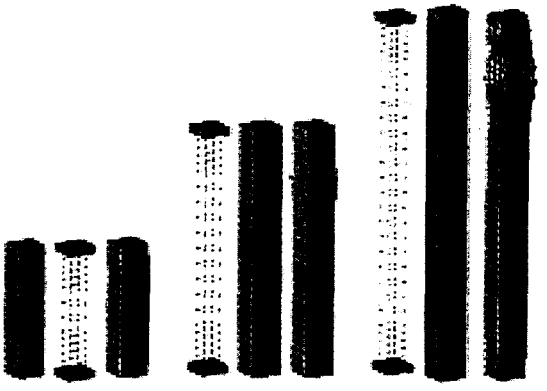

Fig 12- Undeformed and deformed meshes used for the computations on specimensof size D = 12.7 mm (0.5 in.).

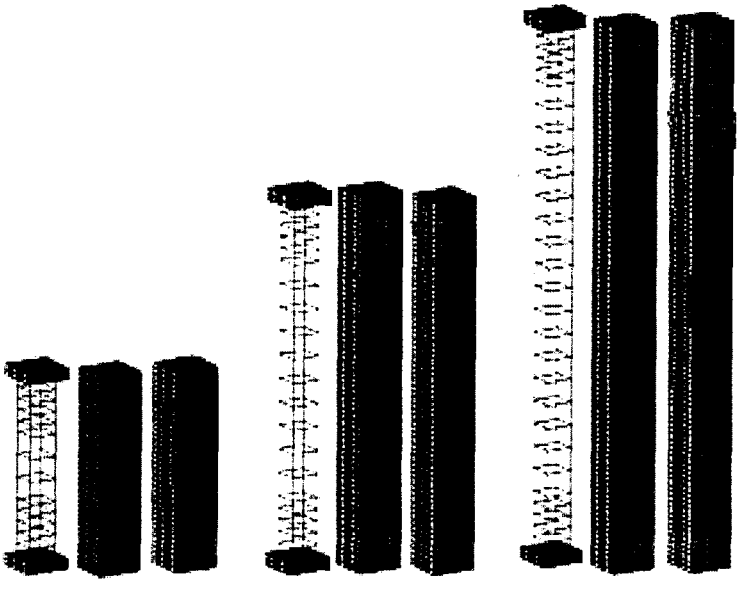

Fig 13- Undeformed and deformed meshes used for the computations on specimens of size D = 25.4 mm (1.0 in.).

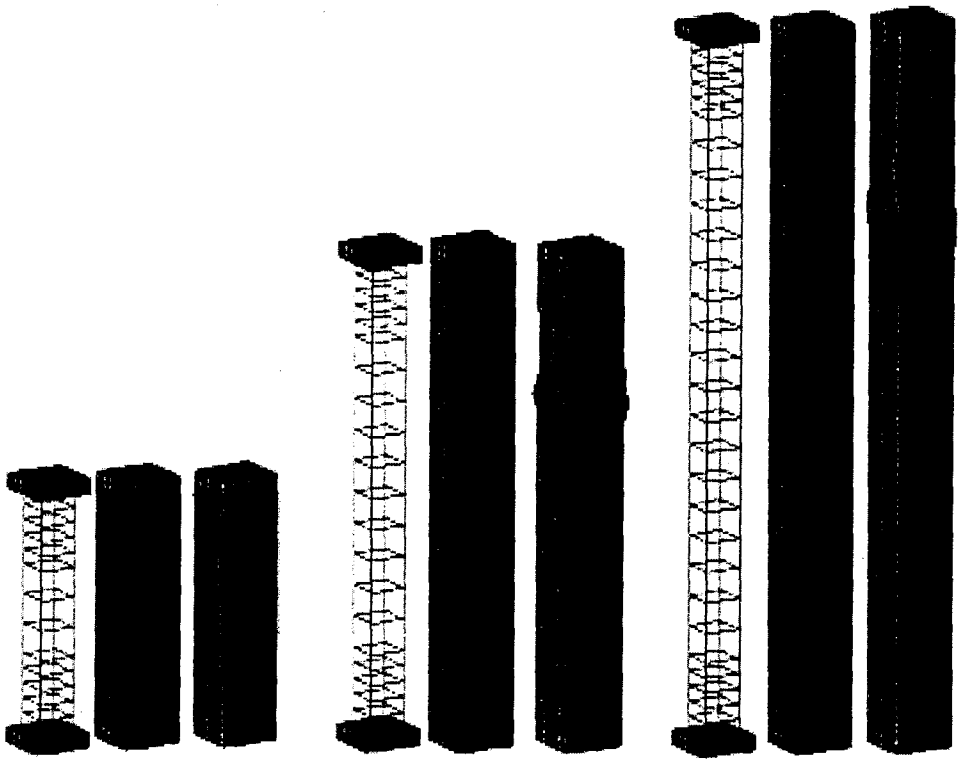

Fig 14- Undeformed and deformed meshes used for the computations on specimens of size D = 50.8 mm (2.0 in.).

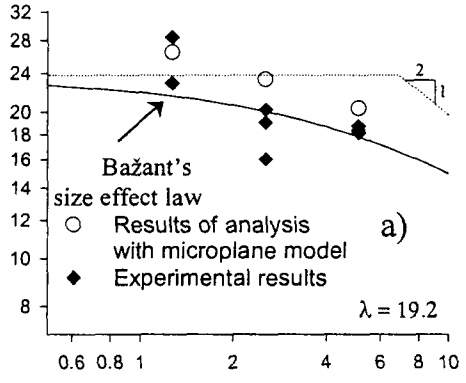

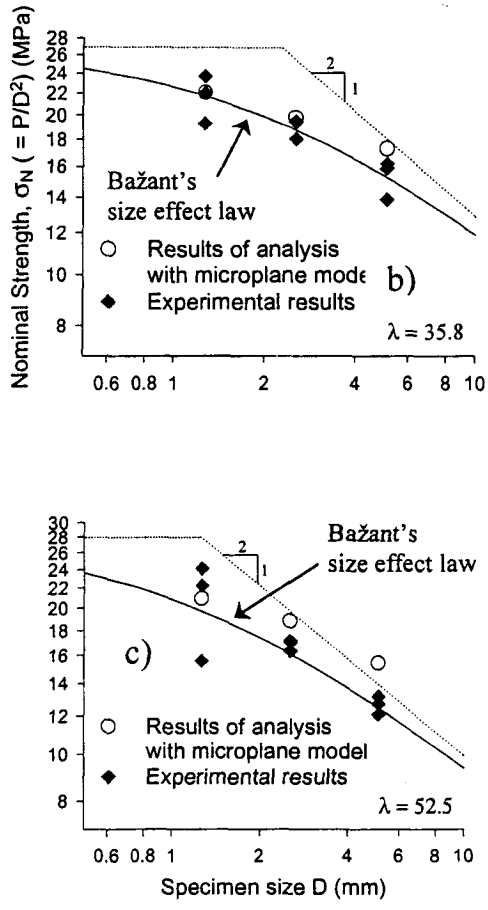

Fig 15- Size effect plots for the specimens with slenderness λ = 19.2 (a), 35.8 (b), 52.5 (c).

6 CONCLUSION

A complete model for compression behavior and failure of concrete must capture (1) compression fracture of strain-softening damage, with the associated size effect, and (2) plastic repsonse under extremely high hydrostatic pressures. The microplane model in its latest version M4, combined with the crack band approach to handle localization in an objective manner, can capture both aspects, as demonstrated by successful simulation of the compressive failure of reinforced concrete columns with the observed size effect and of the tube squash test with shear strains of the order of 100%.

REFERENCES

[1] Bažant, Z.P., Microplane Model for Strain Controlled Inelastic Behavior. Chapter 3 in *Mechanics of Engineering Materials* ed. by C.S. Desai and R.H. Gallagher, J. Wiley, London, 45-59 (1984).

[2] Bažant, Z.P. and Oh, B.H., Efficient Numerical Integration on the Surface of a Sphere. Zeitschrift fur angewandte Mathematik und Mechanik (ZAMM, Berlin),66 (1),37-49 (1986).

[3] Bažant, Z.P. and Prat, P., 1987. Creep of anisotropic clay: new microplane model. ASCE Journal of Engineering Mechanics. 103(7), 1050-1064, (1987).

[4] Bažant, Z.P., and Prat, P.C., "Microplane model for brittle plastic materials: II. Verification" ASCE J. of Engrg. Mechanics Vol. 114, pp. 1689-1702, (1988).

[5] Bažant, Z.P., Caner, F.C., Carol, I., Adley, M.D. and S.A. Akers. Microplane model M4 for concrete: I. Formulation with work-conjugate deviatoric stress. *Report 98-12/407m, Northwestern University*; submitted to *J. of Engrg. Mechanics ASCE*, (1999).

[6] Bažant, Z.P., Caner, F.C., Adley, M.D. and S.A. Akers. Microplane model M4 for concrete: II. Algorithm, calibration and application. *Report 98-12/407m, Northwestern University*; submitted to *J. of Engrg. Mechanics ASCE*, (1999).

[7] Bažant, Z.P., Adley, M.D., Carol, I., Jirasek, M., Akers, S.A., Rohani, B., Cargile J.D. and Caner, F.C. Large-Strain Generalization of Microplane Model for Concrete. *Report 98-12/407l, Northwestern University*; submitted to *J. of Engrg. Mechanics ASCE*, (1999).

[8] Bažant, Z.P., Caner, F.C., Adley, M.D. and S.A. Akers. Incorporation of rate effects of fracturing and creep into microplane model M4 for concrete dynamics. *Report 98-12/407i, Northwestern University*; submitted to *J. of Engrg. Mechanics ASCE*, (1999)

[9] Carol, I. and Bažant,Z.P. Damage and Plasticity in Microplane Theory. *Int. J. of Solids and Structures* 34 (29), 3807-3835, (1997).

[10] Bažant, Z.P. and Oh, B.H. Efficient Numerical Integration on the Surface of a Sphere. *Zeitschrift fur Angewandte Mathematik und Mechanik* (ZAMM, Berlin),66 (1),37-49, (1986).

[11] Stroud, A. H. *Approximate calculation of multiple integrals*. Prentice-Hall, Englewood Cliffs, N. J, (1971).

[12] Bažant, Z.P., Kim, J.J. and M. Brocca. Finite Strain Tube-Squash Test for Concrete at High Pressures and Shear Angles up to 70°. *ACI Materials Journal*, (1999).

[13] Van Mier, J.G.M. Multiaxial strain softening in concrete. *Mat. And Struct.*, 19,179-200, Paris, (1986).

[14] Gonnermann, H.F. Effect of size and shape of test specimen on compressive strength of concrete. *Proc., ASTM*, Philadelphia, Pa., 25, 237-250 (1925).

[15] Blanks, R.F. and McNamara, C.C., Mass concrete tests in large cylinders. J. Am. Concrete Inst., 31, 280-303, (1935).

[16] Marti, P., Size effect on double punch tests on concrete cylinders. ACI Mat. J.,86(6), 597-601, (1989).

[17] Jishan, X., and Xixi, H., Size effect on the strength of a concrete member. Engrg. Fracture Mech., 35, 687-696, (1990).

[18] Nilson, A.H. and Winter, G. *Design of Concrete Structures*. 10th Edn., McGraw-Hill, New York, (1986).

[19] McGregor, J.G. *Reinforced Concrete: Mechanics and Design*. Prentice-Hall, Englewood Cliffs, NJ, (1988).

[20] Bažant, Z.P., and Cedolin, L. *Stability of Structures: Elastic, Inelastic, Fracture and Damage Theories*. Oxford University Press, New York, (1991).

[21] Bažant, Z. P. and Xiang, Y. Size effect in compression fracture: splitting crack band propagation. *J. Engng. Mech. ASCE*, 123(2), 162-172, (1997).

[22] Bažant, Z.P., 1984b. Size Effect in Blunt Fracture: Concrete, Rock, *Metal. J. Engng. Mech. ASCE*, 110, 518-535.

[23] Bažant, Z.P., Cedolin, L. and Tabbara, M.R. New Method of Analysis for Slender Columns. *ACI Struct. J.* 88(4), 391-401, (1991)

[24] Bažant, Z. P., Xi, Y. Statistical size effect in quasi brittle structures: nonlocal theory. *J. Engng. Mech. ASCE*, 117(11), 2623-2640, (1991).

[25] Ingraffea, A.R. *Discrete fracture propagation in rock: laboratory tests and finite element analysis*. PhD dissertation, Univ. of Colorado, Boulder, (1977).

[26] Bažant, Z.P. and F.-B. Lin and H. Lippmann. (1993). Fracture Energy Release and Size Effect in Borehole Breakout. *Int. J. of Num. & Anal. Meth. in Geomech.*, 17, 1-14, (1993).

[27] Bieniawski, Z.T., Estimating the strength of rock materials. *J. S. Afr. Inst. Min. Metal,* 74, 312-320, (1974).

[28] Hoek, E. and Bieniawski, Z.J. Brittle fracture propagation in rock under compression. *Int. J. Fracture Mech.*, 1,137-155, (1965).

[29] Cotterell, B., 1972. Brittle fracture in compression. *Int. J. Fract. Mech.*, 8(2), 195-208, (1972).

[30] Paul, B. Macroscopic criteria for plastic flow and brittle fracture. *Fracture, an advanced treatise*, H. Liebowitz, ed., 2, chapter 4, (1968).

[31] Bažant, Z. P. and Xiang, Y. Size effect in compression fracture: splitting crack band propagation. *J. Engng. Mech. ASCE*, 123(2), 162-172, (1997).

[32] Bažant, Z.P. and Kwon, Y.K. Failure of slender and stocky reinforced concrete columns: tests of size effect. Materials and Structures, 27, 79-90, (1994).

[33] Bažant, Z.P. Instability, Ductility and size effect in strain softening concrete. *J. of the Engineering Mechanics Division, ASCE*, 102, 331-344, (1976).

[34] Bažant, Z. P. and J. Planas. *Fracture and Size Effect in Concrete and Other Quasibrittle Materials*. CRC Press, Boca Raton, Florida, (1998).

[35] Bažant, Z.P. and B.H. Oh. Crack band theory for fracture of concrete. *Mater. Struct.*, 16, 155-177, (1983).

[36] Bažant, Z.P., and Kazemi, M.T. Determination of fracture energy, process zone length and brittleness number from size effect, with application to rock and concrete. *Int. J. Fract.*, 44, 111-131, (1990).

[37] Bažant, Z.P. Recent advances in brittle-plastic compression failure: Damage localization, Scaling and finite strain. *Computational plasticity: Fundamentals and applications* (Proc., 5th Int. Conf. on Comput. Plasticity, COMPLAS 5, held in Barcelona), D. R. J. Owen, E. Onate and E. Hinton, Eds., publ. By Int. Center for Num. Meth. In Engrg., Barcelona, 3-19, (1997).

[38] Bažant, Z.P. Size Effect in Blunt Fracture: Concrete, Rock, *Metal. J. Engng. Mech. ASCE*, 110, 518-535, (1984).

[39] Abusiaf, H.F, Sener, S. and Barr, B.I.G. Size effects in plain and reinforced concrete columns. Report, Div. Of Civil Engrg., Univ. of Wales, Cardiff, U.K, (1996).